ADVANCED HEALTHCARE MATERIALS

Supporting Information

for *Adv. Healthcare Mater.*, DOI 10.1002/adhm.202402431

Eumelanin-Enhanced Photothermal Disinfection of Contact Lenses Using a Sustainable Marine Nanoplatform Engineered with Electrospun Nanofibers

*Magdalena Bartolewska, Alicja Kosik-Kozioł, Zbigniew Korwek, Zuzanna Krysiak, Devis Montroni, Maciej Mazur, Giuseppe Falini and Filippo Pierini**

Supporting Information

Eumelanin-Enhanced Photothermal Disinfection of Contact Lenses Using a Sustainable Marine Nanoplatform Engineered with Electrospun Nanofibers.

*Magdalena Bartolewska, Alicja Kosik-Kozioł, Zbigniew Korwek, Zuzanna Krysiak, Devis Montroni, Maciej Mazur, Giuseppe Falini and Filippo Pierini**

M.Bartolewska, Dr. A.Kosik-Kozioł, Dr. Z Korwek, Dr. Zuzanna Krysiak, Prof. F. Pierini
Department of Biosystems and Soft Matter, Institute of Fundamental Technological Research, Polish Academy of Sciences, Warsaw, 02-106, Poland
E-mail: fpierini@ippt.pan.pl

Prof. M. Mazur
Department of Chemistry, University of Warsaw, Warsaw, 02-093, Poland

Dr. D. Montroni, Prof. G. Falini
Dipartimento di Chimica "G. Ciamician", Alma Mater Studiorum—Università di Bologna, via F. Selmi 2, 40126 Bologna, Italy

Figure S1 shows the SEM images of the mussel shell structure, highlighting three distinct layers: the periostracum layer (PL), the prismatic layer (PRL), and the nacre layer (NL). The periostracum layer serves as the outermost protective layer, composed primarily of organic materials (14 µm). Beneath this lies the prismatic layer (250 µm), consisting of calcite crystals arranged in a prismatic structure, providing rigidity and support. The innermost nacre layer (125 µm), known for its iridescent properties, is composed of aragonite platelets and organic matrix, offering both strength and toughness through its unique microarchitecture.

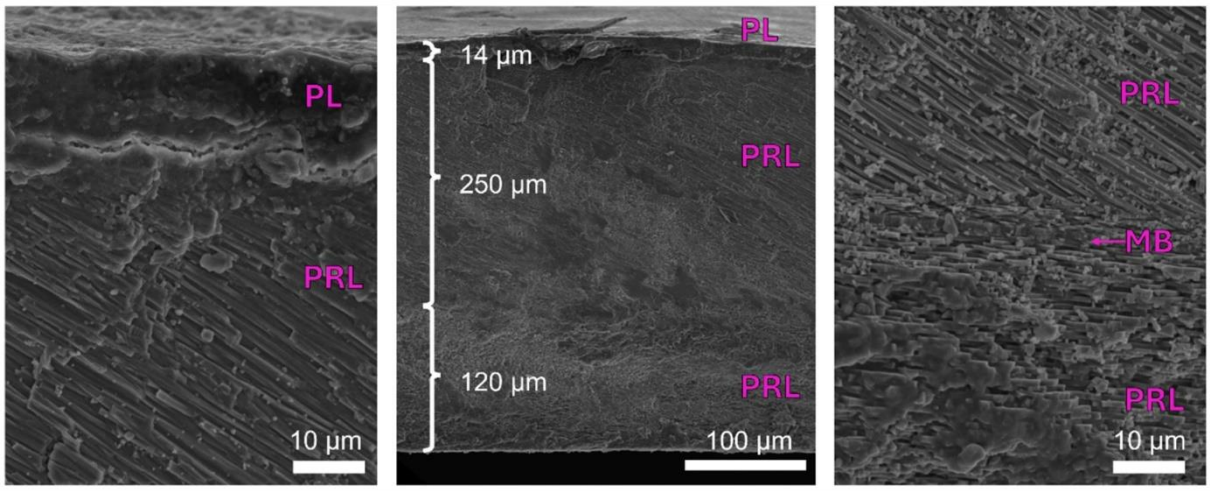

Figure S1. SEM of mussel shell structure. periostracum layer - PL, prismatic layer - PRL, myostracum barrier - MB, nacre layer - NL.

Figure S2 illustrates the Raman spectra of the prismatic and nacre layer from mussel shells both before and after the demineralization process. In the Raman spectrum of the prismatic and nacre layer from the mussel shell ((PRL+NL)MS), distinct lattice modes are observed at 155 and 206 cm^{-1}, alongside internal modes at 704 and 1085 cm^{-1}, indicative of calcium carbonate's characteristics. These characteristic peaks are notably absent in the prismatic and nacre layer of the demineralized mussel shell ((PRL+NL)deMS), confirming the effectiveness of the demineralization process. Additionally, polyene-related Raman peaks at 1105 and 1486 cm^{-1} are present in both the mineralized and demineralized layers, although their intensity shows significant variation post-demineralization.

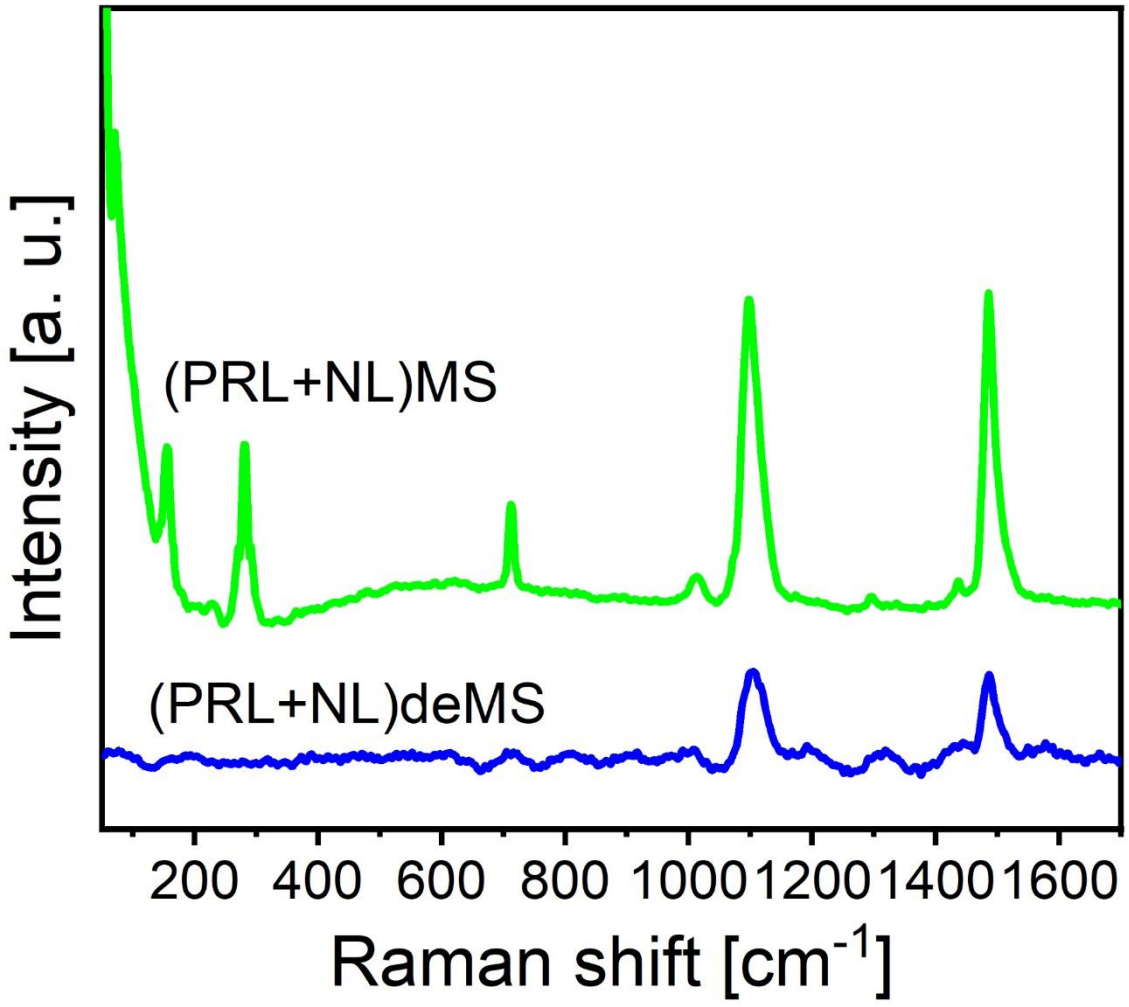

Figure S2. Raman spectra of mussel shell pre- and post-demineralization.

Figure S3 illustrates the SEM images of nanofibers with varying concentrations of 0.1% chitin nanofibrils in acetic acid (CT) solution in a 10% polyvinyl alcohol (PVA) matrix. The images detail the morphological changes as the CT content increases:

(a) PVA/CT (10:0; v/v): pure PVA nanofibers exhibit a smooth, uniform structure.

(b) PVA/CT (9:1; v/v): the introduction of CT did not result in changes to the fiber morphology.

(c) PVA/CT (7:3; v/v): increased CT content begins to show minor roughness on the fiber surfaces.

(d) PVA/CT (5:5; v/v): equal parts PVA and CT result in significant roughening and structural irregularities in the nanofibers.

(e) PVA/CT (4:6; v/v): a high concentration of CT results in the formation of numerous beads.

These variations indicate that CT integration into PVA affects the fibers formation process, impacting their structural properties and, potentially, their functional characteristics.

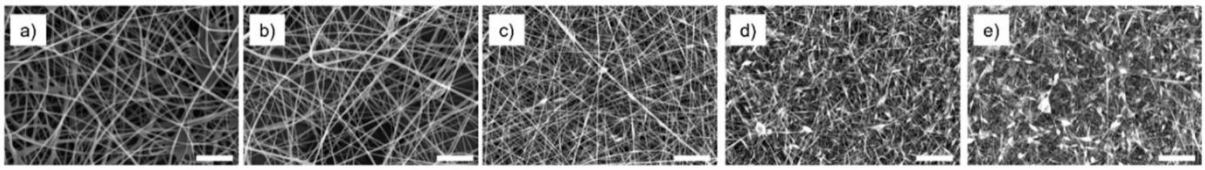

Figure S3. SEM of nanofibers with increasing amounts of CT solution in 10% PVA nanofibers. (a) PVA/CT (10:0; v/v) (b) PVA/CT (9:1; v/v) (c) PVA/CT (8:2; v/v) (d) PVA/CT (7:3; v/v) (e) PVA/CT (5:5; v/v). Scale bar: 10 µm.

The comparison in Figure S3 highlights the influence of PEO in modulating the fiber characteristics, producing beadless fibers.

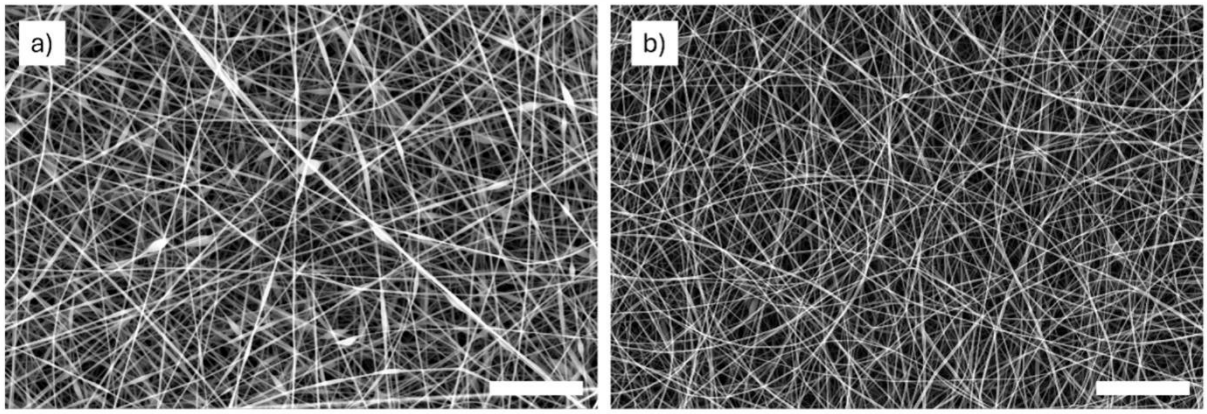

Figure S4. SEM of nanofibers a) 10% (w/v) PVA with CT in ratio (7:3; v/v) b) 10% of PVA/PEO (w/v) with CT in ratio (7:3; v/v). Scale bar: 10 µm.

The presence of holes in the nacre layer (Figure S4) suggests that the crosslinking process, particularly when performed at elevated temperatures, can significantly affect the structural integrity of the nacre layer. Comparable findings were reported in the study by Ji et al., where holes appeared after exposure to 300°C. However, their study also demonstrated that, despite the high temperatures, proteins in the organic matrix were well preserved.[1]

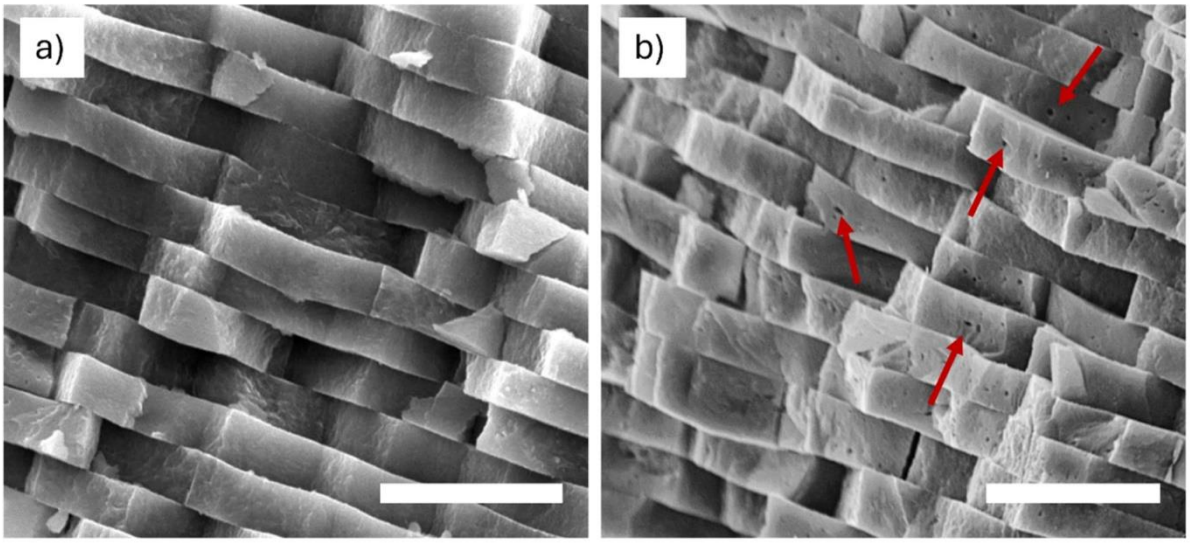

Figure S5. SEM of NL a) before crosslinking, b) after crosslinking with ethanol and temperature. (Red arrows highlight holes). Scale bar: 5 µm.

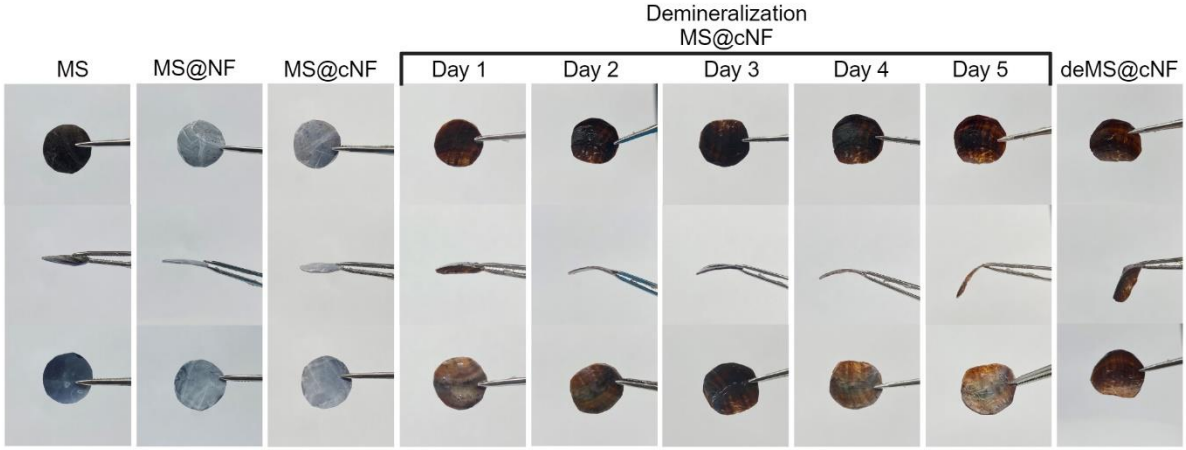

Figure S6. Photographs illustrating the progressive demineralization of the deMS@cNF nanoplatform, showcasing the material's increasing flexibility with each stage.

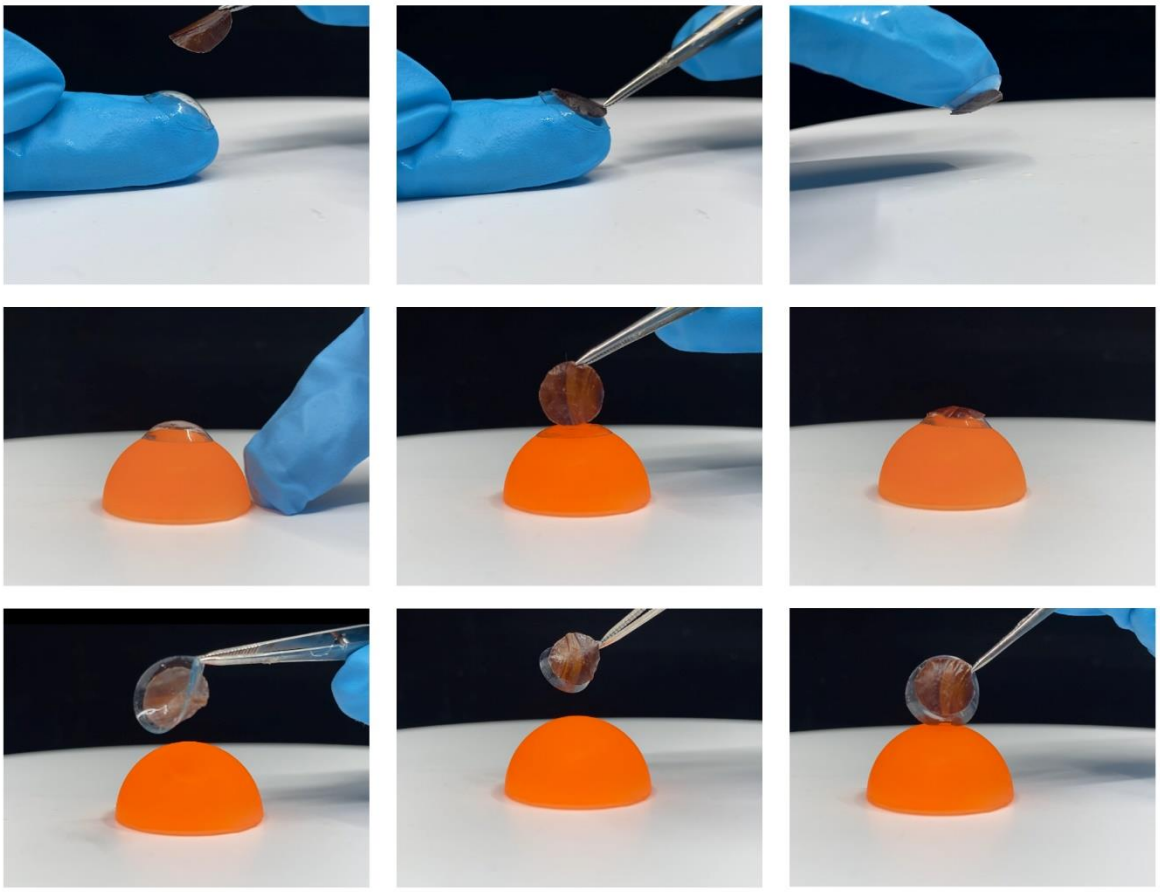

Figure S7. Photographs demonstrating the flexibility of the deMS@cNF nanoplatform and its attachment to the contact lenses.

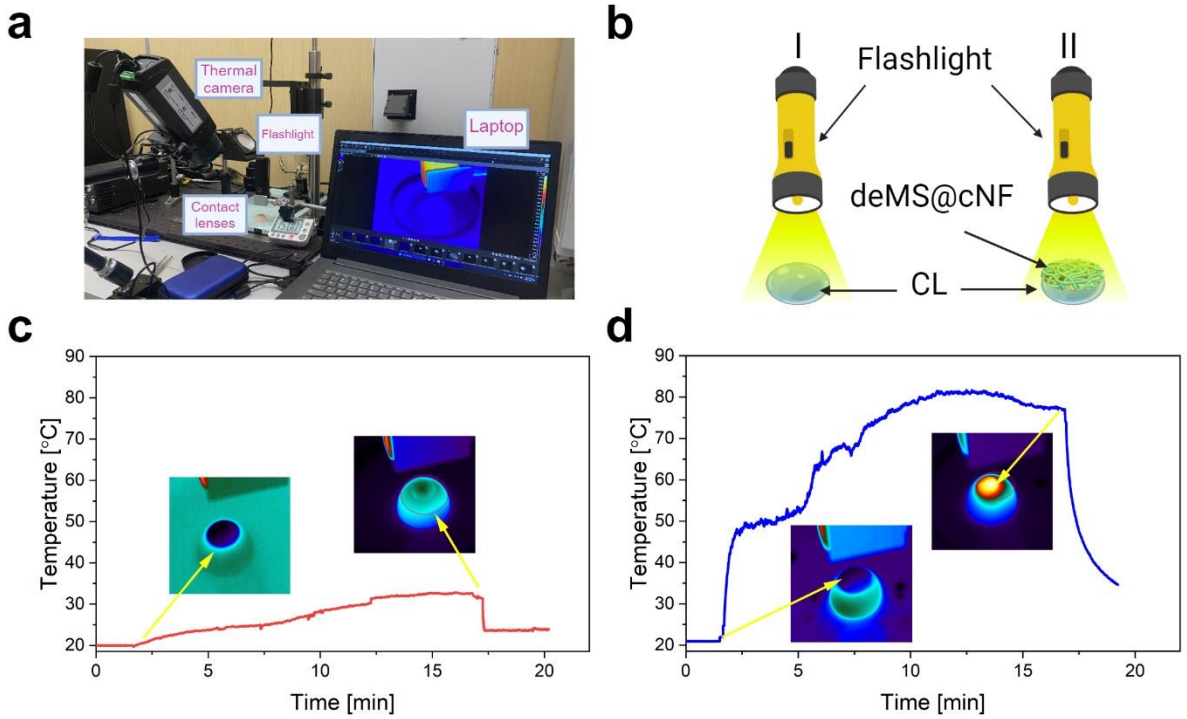

Figure S8. Photothermal Sterilization of Contact Lenses Using a Nanoplatform a) photograph of the disinfection setup, including the thermal camera, flashlight, and contact lenses connected to a laptop for temperature monitoring. b) illustration of irradiation with a flashlight, showing two states: I) contact lenses without the nanoplatform (CL), and II) contact lenses covered with the deMS@cNF nanoplatform. c) time-temperature graph with thermal images for scheme I (contact lens alone), showing temperature no increase and stabilization. d) time-temperature graph with thermal images for scheme II (contact lens with nanoplatform), showing temperature increase and stabilization.

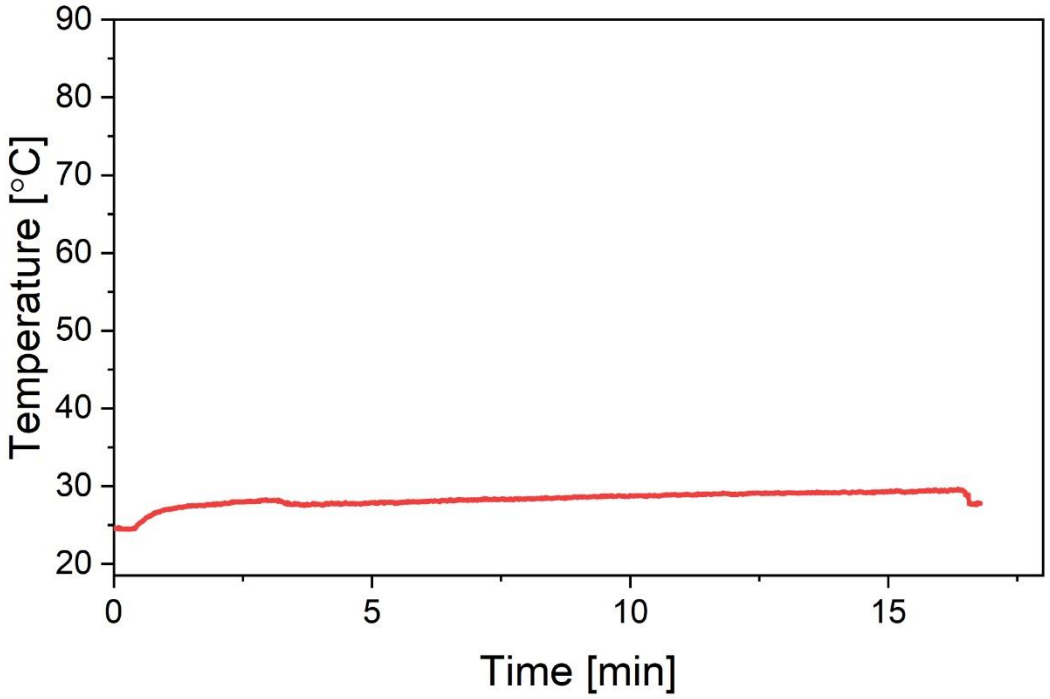

Figure S9. Average time-temperature graph for antibacterial test for irradiation of flashlight on contact lenses (CL+).

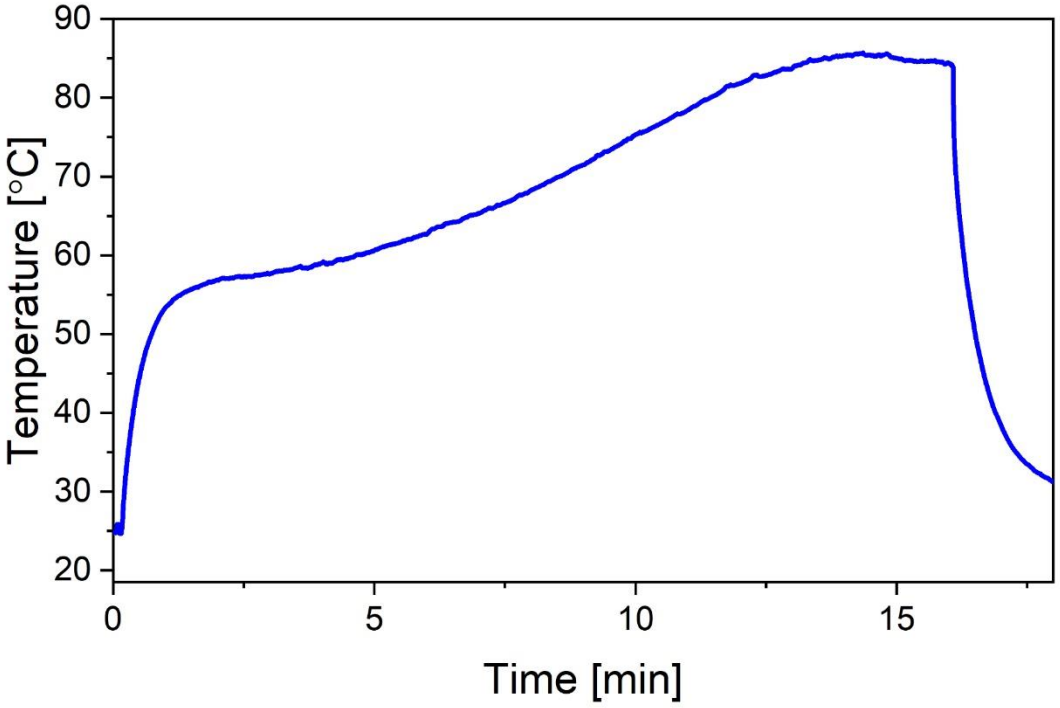

Figure S10. Average time-temperature graph for antibacterial test for irradiation of flashlight on contact lenses with deMS@cNF (CL@D+).

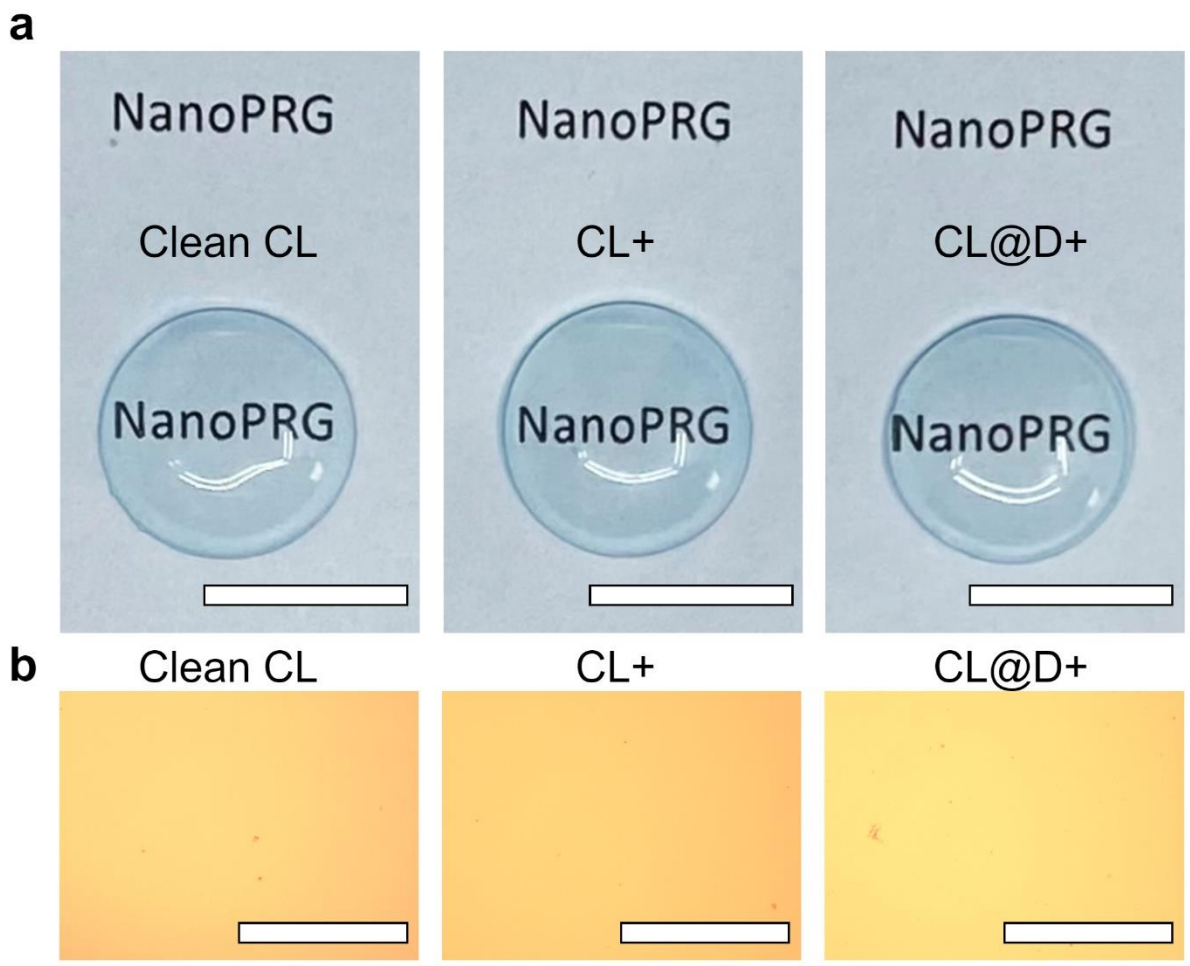

Figure S11. Surface analysis of contact lenses after treatment with DeMS@cNF and flashlight a) photos of contact lenses. Scale bar: 1 cm b) images from light microscope. Scale bar: 12 mm.

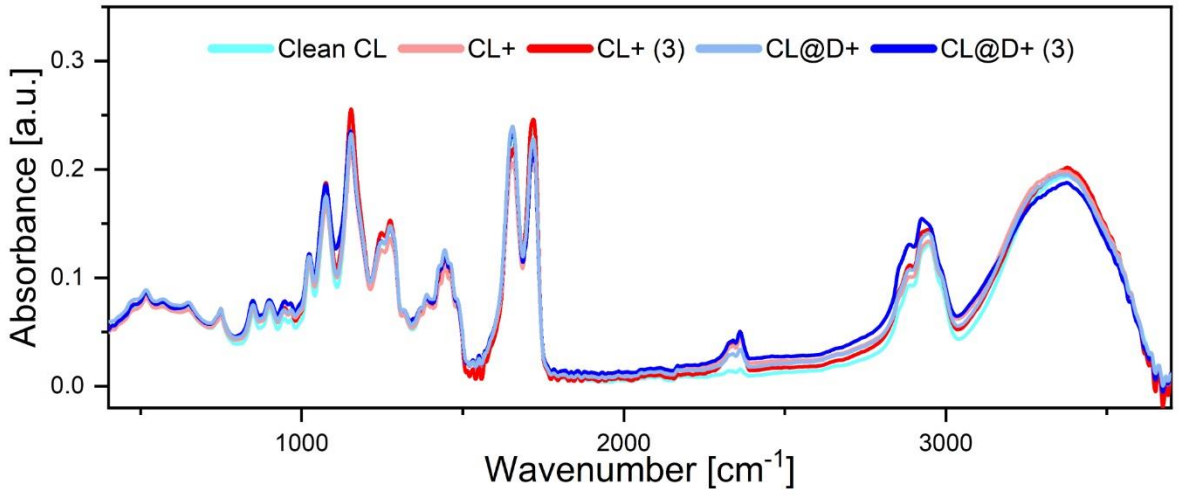

Figure S12. FTIR spectra of contact lenses after treatment with flashlight and with nanoplatform and flashlight. The spectra include Control contact lenses (Clean CL), contact lenses after irradiation with flashlight (CL+), contact lenses after irradiation with flashlight for 3 cycles (CL+ (3)), contact lenses after irradiation with deMS@cNF and flashlight (CL@D+), and contact lenses after irradiation with deMS@cNF and flashlight for 3 cycles (CL@D+ (3)).

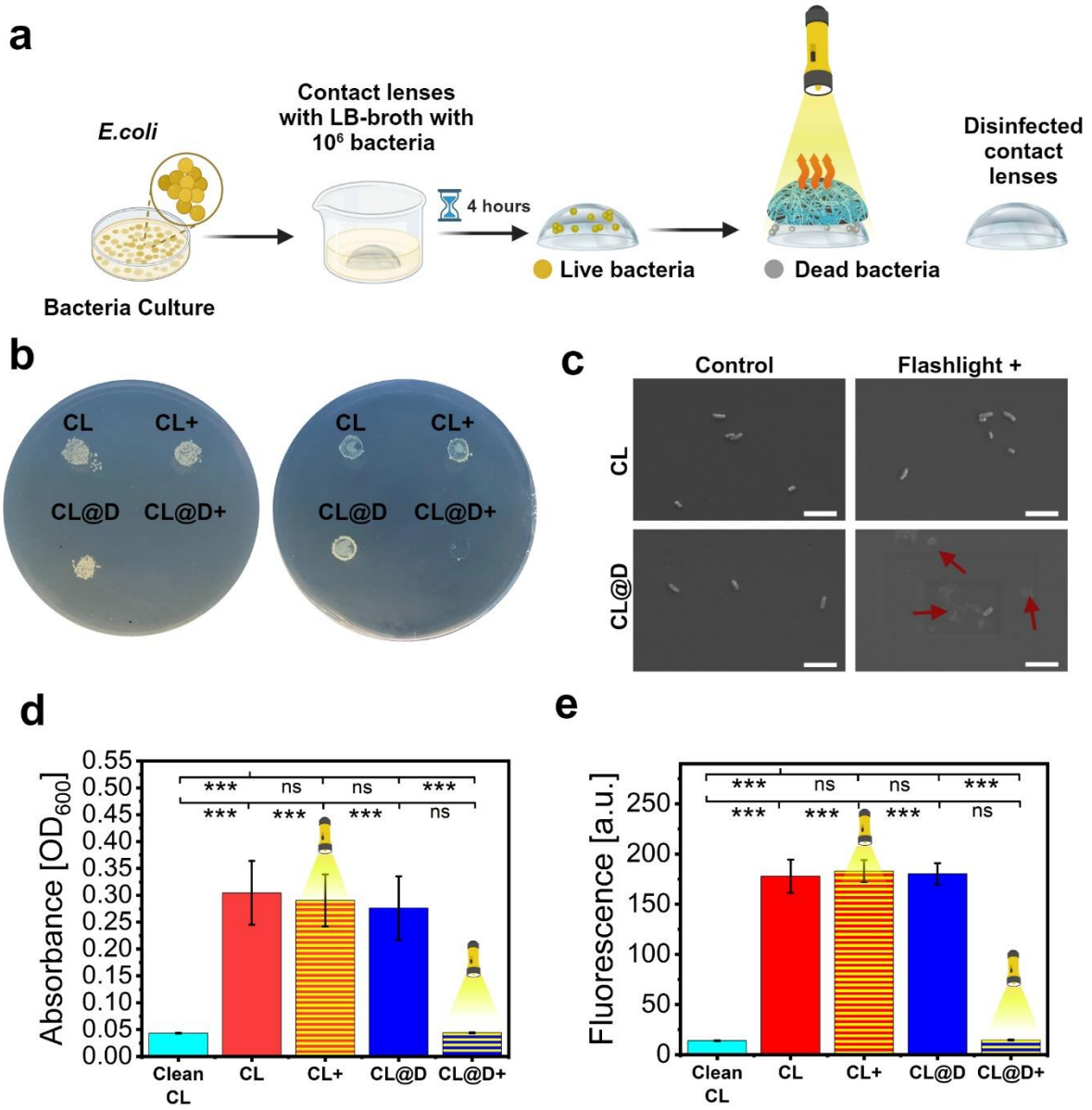

Figure S13. On demand antibacterial studies on contact lenses. a) Illustration of the application of the multifunctional nanoplatform (deMS@cNF) in effectively eradicating bacteria (*E.coli*) from the surface of contact lenses. b) Agar plates showing imprints of irradiated and non-irradiated with and without deMS@cNF contact lenses. c) SEM images of contact lens surfaces contaminated with bacteria before and after flashlight irradiation (+), both with (CL@D) and without (CL) deMS@cNF. Scale bar: 5 µm. d) Optical density measured at 600 nm absorbance after immersing contact lenses overnight in fresh broth. e) Measurement of fluorescence for the PrestoBlue test performed on solutions after overnight soaking of contact lenses. Contact lenses (CL), Contact lenses irradiated with flashlight (CL+), Contact lenses cover with deMS@CNF (CL@D), Contact lenses with deMS@cNF irradiated with flashlight (CL@D+).

List of tables

Table S1. Marine derived photothermal agent for antibacterial application.

Melanin Source	Type of Irradiation	Source Power Density [W/cm^2]	Max Temp. [°C]	Time to Reach Maximum Temperature [min]	Application	Year	Ref
Mussel shell	White LED light	0.32	95	<1	Disinfection of contact lenses	2024	This paper
Cuttlefish ink	NIR light (808 nm)	1	63.6	4	Drug delivery, Wound healing of infected wounds	2024	[2]
Cuttlefish ink	NIR light (808 nm)	0.9	60	10	Wound healing of infected wounds	2024	[3]
Cuttlefish ink	NIR light (808 nm)	1	55	25	Wound healing of infected wounds	2023	[4]
Cuttlefish ink	NIR light (808 nm)	2	70	1	Antibacterial food packaging	2023	[5]
Cuttlefish ink	NIR light (808 nm)	0.2	73	2	Skin Tumor Photothermal Therapy and Wound Healing	2022	[6]

Reference

[1] X. Ji, J. Huang, Z. Wang, Z. Xu, C. Liu, *Front. Mar. Sci.* **2022**, *9*, DOI 10.3389/fmars.2022.850120.

[2] Q. Jia, Z. Fu, Y. Li, Z. Kang, Y. Wu, Z. Ru, Y. Peng, Y. Huang, Y. Luo, W. Li, Y. Hu, X. Sun, J. Wang, Z. Deng, C. Wu, Y. Wang, X. Yang, *ACS Appl. Mater. Interfaces* **2024**, *16*, 13422.

[3] X. Cao, L. Sun, D. Xu, S. Miao, N. Li, Y. Zhao, *Adv Sci (Weinh)* **2023**, *10*, e2300902.

[4] X. Kong, H. Chen, F. Li, F. Zhang, Y. Jiang, J. Song, Y. Sun, B. Zhao, J. Shi, *Int. J. Biol. Macromol.* **2023**, *237*, 124176.

[5] Y. Liang, Y. Han, J. Dan, R. Li, H. Sun, J. Wang, W. Zhang, *Food Res. Int.* **2023**, *163*, 112211.

[6] Q. Lei, D. He, L. Ding, F. Kong, P. He, J. Huang, J. Guo, C. J. Brinker, G. Luo, W. Zhu, Y. Yu, *Adv. Funct. Mater.* **2022**, *32*, DOI 10.1002/adfm.202113269.